PNAS RESEARCH ARTICLE | BIOCHEMISTRY BIOPHYSICS AND COMPUTATIONAL BIOLOGY OPEN ACCESS

# Cholesterol in the cargo membrane amplifies tau inhibition of kinesin-1-based transport

Qiaochu Li[a], James T. Ferrare[b], Jonathan Silver[b], John O. Wilson[a], Luis Arteaga-Castaneda[a], Weihong Qiu[c], Michael Vershinin[d], Stephen J. King[e], Keir C. Neuman[b], and Jing Xu[a,1]

Edited by Kristen J. Verhey, University of Michigan Medical School, Ann Arbor, Michigan; received July 23, 2022; accepted December 8, 2022 by Editorial Board Member Yale E. Goldman

**Intracellular cargos are often membrane-enclosed and transported by microtubule-based motors in the presence of microtubule-associated proteins (MAPs). Whereas increasing evidence reveals how MAPs impact the interactions between motors and microtubules, critical questions remain about the impact of the cargo membrane on transport. Here we combined in vitro optical trapping with theoretical approaches to determine the effect of a lipid cargo membrane on kinesin-based transport in the presence of MAP tau. Our results demonstrate that attaching kinesin to a fluid lipid membrane reduces the inhibitory effect of tau on kinesin. Moreover, adding cholesterol, which reduces kinesin diffusion in the cargo membrane, amplifies the inhibitory effect of tau on kinesin binding in a dosage-dependent manner. We propose that reduction of kinesin diffusion in the cargo membrane underlies the effect of cholesterol on kinesin binding in the presence of tau, and we provide a simple model for this proposed mechanism. Our study establishes a direct link between cargo membrane cholesterol and MAP-based regulation of kinesin-1. The cholesterol effects uncovered here may more broadly extend to other lipid alterations that impact motor diffusion in the cargo membrane, including those associated with aging and neurological diseases.**

membrane fluidity | diffusion | microtubule binding | vesicle transport | motile fraction

## Significance

Kinesin-1 drives long-range vesicle transport along microtubules in eukaryotic cells. Tau is essential for microtubule assembly and stabilization but occludes kinesin-binding sites. In cells, kinesins are often attached to vesicle cargos via a fluid lipid membrane. Here we employ in vitro optical trapping to determine how a lipid cargo membrane affects kinesin-based transport in the presence of tau. We show that tau-inhibition of kinesin is tuned by cholesterol in the cargo membrane. Our results provide insight into how kinesin-based vesicle transport is maintained under tau-enriched conditions such as those found in neurons. Moreover, our results identify cargo membrane cholesterol as a potential therapeutic target to mitigate transport dysfunctions that are a common early hallmark of aging and neurodegeneration.

Kinesin-1 is a major microtubule-based motor protein responsible for long-range transport in eukaryotic cells (1, 2). Underscoring the critical importance of kinesin in cell function and survival, mutations in the neuronal kinesin heavy chain isoform 5A (Kif5A) cause neurodegenerative diseases including hereditary spastic paraplegias (3), Charcot-Marie-Tooth disease type 2 (4), and amyotrophic lateral sclerosis (5). Kinesin transports cargos by processively stepping along microtubules (6, 7); this processive motion is initiated when the motor binds the microtubule and is terminated when it unbinds from the microtubule. Tuning of the binding and unbinding rates of kinesin, for example via the presence of microtubule-associated proteins (MAPs) (8–10), has emerged as a key mechanism of kinesin regulation. In particular, the MAP tau occludes kinesin-binding sites on the microtubule (10–12), inhibiting binding and promoting unbinding of kinesin in vitro (13–15). However, in vivo, tau is essential for microtubule assembly and stabilization (16). How kinesin maintains transport in the presence of tau, particularly in environments such as healthy neurons where tau is enriched, remains to be elucidated.

In cells, kinesins are often attached to their cargos via a fluid lipid membrane (17–19). This cargo-enclosing membrane is absent from most in vitro investigations, including the pioneering studies that established tau inhibition of kinesin-based transport (13–15). The lipid membrane enclosing cargos in vivo is "fluid" in that its constituents, including motor proteins such as kinesin, are mobile and can diffuse on the cargo surface. As membrane fluidity increases, each motor protein can more quickly diffuse to open binding sites on the microtubule via diffusive search. Alterations in membrane cholesterol or other fluidity-restricting lipids are increasingly linked to aging and neurological diseases (20, 21), in which dysfunctions in motor-based transport have emerged as a common early hallmark (22). These in vivo observations suggest that diffusion of motors in the cargo membrane may contribute to transport regulation. However, recent investigations found no significant effects of a lipid membrane (23, 24) on the binding or unbinding rates of kinesins to microtubules in the absence of MAPs.

Here we employed in vitro optical trapping to determine how a lipid cargo membrane affects kinesin-based transport in the presence of the MAP tau. We generated membrane-enclosed cargos by enclosing silica microspheres with a fluid lipid bilayer (23, 25–27). We first compared the transport of membrane-enclosed cargos with that of membrane-free cargos, for which tau inhibition of kinesin-based transport is well-established (14, 28). We then examined whether adding cholesterol to the lipid bilayer, which reduces

Author contributions: Q.L. and J.X. designed research; Q.L., J.T.F., J.S., L.A.-C., K.C.N., and J.X. performed research; Q.L., J.O.W., M.V., and J.X. analyzed data; W.Q., M.V., and S.J.K. contributed new reagents/analytic tools; and M.V., K.C.N., and J.X. wrote the paper.

The authors declare no competing interest.

This article is a PNAS Direct Submission. K.J.V. is a guest editor invited by the Editorial Board.



[1]To whom correspondence may be addressed. Email: jxu8@ucmerced.edu.

This article contains supporting information online at https://www.pnas.org/lookup/suppl/doi:10.1073/pnas.2212507120/-/DCSupplemental.

Published January 10, 2023.

membrane fluidity and kinesin diffusion in the cargo membrane (24, 27, 29), impacted the transport of membrane-enclosed cargos. Importantly, the concentration of kinesin was kept constant across cholesterol levels, enabling direct comparison of membrane-enclosed cargos with the same numbers of attached motors (*Materials and Methods*). We next developed theoretical models providing quantitative measures of individual motor binding and mechanistic insight into our in vitro findings. Together, our experimental and theoretical results establish a direct link between cargo membrane cholesterol and MAP-based regulation of kinesin-1.

## Results

**A Fluid Lipid Membrane Reduces the Inhibitory Effect of tau on Kinesin-1.** We first compared the transport of membrane-enclosed versus membrane-free cargos. We used a cholesterol-free, dioleoylphosphatidylcholine (DOPC) lipid bilayer to model the fluid membrane of intracellular cargos (26, 30, 31), and we included biotinylated or nickel-loaded chelator lipids in the bilayer to mediate kinesin attachment (Table 1). We employed human tau 23 (htau23, or 3RS tau), an isoform of tau that strongly inhibits kinesin in vitro (13–15), and we characterized cargo transport by ~1 to 2 kinesins as observed for intracellular vesicles (17–19). Because it is difficult to definitively match the numbers of attached kinesins on the two classes of cargos, we designed our experiments to empirically match a key transport characteristic ("motile fraction"; Fig. 1*A*, *Inset*) in the absence of tau. We then determined the effect of tau for each class of cargos in comparison to this matched tau-free baseline. Since tau inhibition of kinesin is well established in vitro for the ubiquitous kinesin heavy chain isoform 5B (Kif5B) (13, 15), we assayed the effect of a DOPC membrane on Kif5B-based transport in addition to the neuronal isoform Kif5A, mutations in which cause neurodegeneration (3–5).

To quantify transport, we used a custom-built optical trap to position individual kinesin–cargo complexes near a microtubule for up to 30 s (Fig. 1*A*, *Inset*; and Movie S1); in the absence of tau, this 30-s interaction time is sufficient for binding if there is active kinesin on the cargo (6, 32, 33). We scored the fraction of cargos that bound to, and moved along, the microtubule ("motile fraction"). For cargos that were motile, we turned off the optical trap and measured the distance that the cargo traveled before unbinding from the microtubule ("run length"). Both motile fraction and run length impact the flux of cargos transported in vivo.

Attaching kinesins to a fluid lipid membrane reduced the inhibitory effect of tau on motile fraction for both the ubiquitous isoform Kif5B and the neuronal isoform Kif5A (Fig. 1, *Top*). We empirically tuned the concentration of motors in each cargo preparation to match the motile fraction for membrane-enclosed and membrane-free cargos in the absence of tau (~75%; Fig. 1*A*, *Top*). This motile fraction corresponds to ~30% of motile cargos being carried by two or more kinesins (34), mimicking the in vivo scenario (17–19). For the ubiquitous isoform Kif5B, the motile fraction of both membrane-free and membrane-enclosed cargos decreased with increasing concentrations of tau (Fig. 1*A*, *Top*). This result is consistent with prior reports that tau reduces the binding rate of kinesin for the microtubule (13–15). However, in contrast to membrane-free cargos (gray, Fig. 1*A*, *Top*), the motile fraction of membrane-enclosed cargos was less impacted by tau (blue, Fig. 1*A*, *Top*), suggesting that diffusion of kinesins in the fluid cargo membrane may improve kinesin binding in the presence of tau. Similarly, for the neuronal isoform Kif5A, the motile fraction was significantly higher for membrane-enclosed cargos than membrane-free cargos in the presence of tau (blue, Fig. 1*B*, *Top*). To control for the possibility that the cargo membrane removes tau from the microtubule, we repeated motile-fraction measurements using microtubules preincubated with excess DOPC lipid vesicles. Consistent with reports that tau binds anionic but not neutral lipids (35), preincubating microtubules with neutral DOPC lipid vesicles did not impact motile-fraction measurements (*SI Appendix*, Fig. S1).

The effect of a fluid membrane on cargo run length differed between the two kinesin isoforms (Fig. 1, *Bottom* and *SI Appendix*, Figs. S2 and S3). We confirmed that a fluid DOPC membrane did not impact cargo run length in the absence of tau (Fig. 1*A*, *Bottom*; and ref. 23). Note that these tau-free run lengths were not substantially longer than that of a single kinesin (*SI Appendix*, Figs. S2 and S4*A* for Kif5B and *SI Appendix*, Figs. S3 and S4*B* for Kif5A). This result is consistent with our previous reports (23, 34) and reflects the fact that, at the ~75% motile fraction examined here, the majority of motile cargos are carried by a single kinesin (6, 32, 34). We also verified that the run lengths of both isoforms decreased in the presence of tau (Fig. 1, *Bottom*; and refs. 14, 15, and 36). For the ubiquitous isoform Kif5B, cargo run length was less impacted by tau when the motors were membrane-bound (Fig. 1*A*, *Bottom*). In contrast, for the neuronal isoform Kif5A, there was no significant difference in tau's effects on the run length of membrane-enclosed cargos and membrane-free cargos (Fig. 1*B*, *Bottom*). A key difference between the isoforms is that Kif5A unbinds from the microtubule substantially faster than Kif5B (*SI Appendix*, Fig. S4), which in general reduces the sensitivity of cargo run length to the motor's microtubule-binding rate or changes thereof (37, 38). Hereafter, we focused our study on the neuronal isoform Kif5A based on its significance in neuronal physiology and human health (3–5).

**Table 1. Membrane lipid compositions.**

| Type of lipid | Membrane A (mol%) | Membrane B (mol%) | Membrane C (mol%) | Membrane D (mol%) |
|---|---|---|---|---|
| DOPC | 95 | 95 | 70 | 55 |
| Cholesterol | – | – | 25 | 50 |
| DSPE-PEG(2000) Biotin | 5 | – | – | – |
| 18:1 DGS-NTA(Ni) | – | 5 | 5 | 5 |

DOPC: dioleoylphosphatidylcholine, a neutral lipid that models the fluid membrane of intracellular cargos (30, 31). DSPE-PEG(2000) Biotin: 1,2-distearoyl-sn-glycero-3-phosphoethanolamine-N-[biotinyl(polyethylene glycol)-2000] (ammonium salt), a biotinylated lipid that mediates the attachment of the kinesin-1 heavy chain isoform 5B (residues 1 to 560, C-terminal biotin tag). 18:1 DGS-NTA(Ni): 1,2-dioleoyl-sn-glycero-3-[(N-(5-amino-1-carboxypentyl)iminodiacetic acid)succinyl] (nickel salt), a nickel-loaded chelator lipid that mediates the attachment of the kinesin-1 heavy chain isoform 5A (full-length, C-terminal hexahistidine tag).

**Membrane Cholesterol Amplifies the Inhibitory Effect of tau on Kinesin-1.** Our data in Fig. 1 suggest that motor diffusion in the cargo membrane may impact kinesin binding in the presence of tau. Comparisons of membrane-free cargos and membrane-enclosed cargos, however, are complicated by potential differences in the numbers of attached motors on the two classes of cargos, as well as uncertainties regarding the rotational diffusion of membrane-free cargos. Whereas it is generally assumed that an optically trapped bead rotates freely and isotropically, this assumption has not been validated and is directly contradicted by experiments (39, 40). We therefore focused our investigations on measurements of membrane-enclosed cargos that employed identical motor attachment and differed only in their cholesterol content.

We added up to 50 mol% cholesterol to our cargo membrane (Table 1). This range of cholesterol addition is within its solubility limit of ~67 mol% in phosphatidylcholine lipids (41, 42), reducing

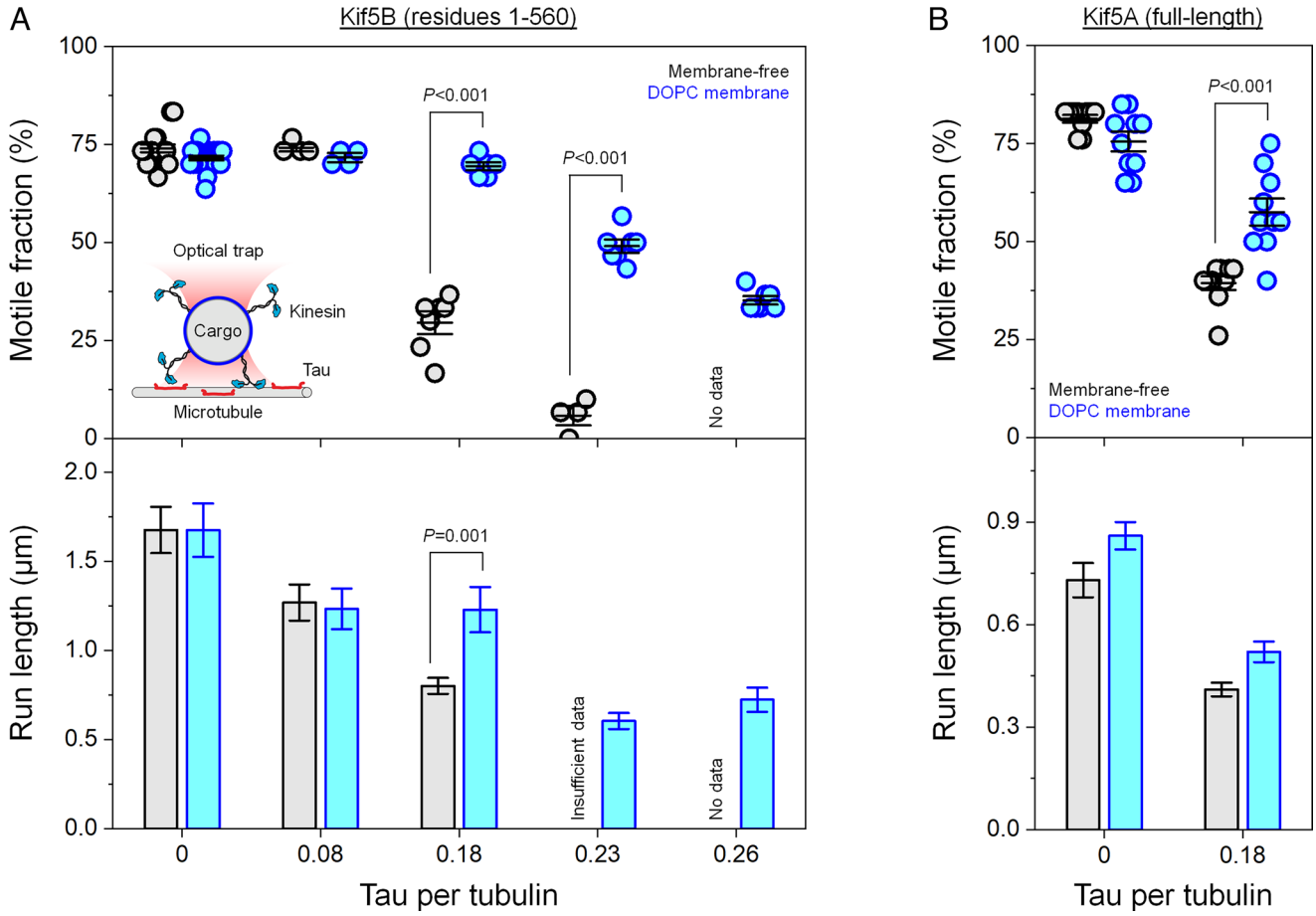


**Fig. 1.** A fluid lipid membrane reduces the inhibitory effect of tau on kinesin-1. (*A*) Transport of membrane-free (gray) and membrane-enclosed (blue) cargos by the ubiquitous kinesin heavy chain isoform Kif5B, as a function of tau concentration (represented as the incubation ratio of tau per tubulin dimer). For each cargo type, the concentration of kinesin used to prepare the motor–cargo complex was empirically tuned to achieve the same motile fraction on tau-free microtubules (~75%) and kept constant across all tau concentrations (*Materials and Methods*). *Inset*: Experimental schematic (not to scale). An optical trap confines an individual cargo near the microtubule. A motile event is scored if the cargo displays directed motion within 30 s. The trap is then shuttered to measure the zero-load run length. A representative movie of nonmotile cargo is provided in Movie S1. *Top*: Motile fraction of cargos. Horizontal lines indicate mean and 68% CI. $n$ = 4 to 22 trials, with 30 cargos measured in each trial. Significant $P$-values from two-sample Welch's $t$ tests are indicated. *Bottom*: Mean run length of motile cargos. Error bars indicate SEM. $n$ = 50 to 419 motile runs for the indicated mean run lengths. Low motile fractions of membrane-free cargos (<5%) at higher tau concentrations (0.23 and 0.26 tau per tubulin) resulted in insufficient data ($n$ = 6 runs) or no data ($n$ = 0 runs) for run-length determination. Mann–Whitney $U$ tests returned one significant $P$-value. Run-length distributions are provided in *SI Appendix*, Fig. S2. (*B*) Cargo transport by the neuronal kinesin heavy chain isoform Kif5A, for two tau concentrations. CIs and error bars are as described in (*A*). *Top*: $n$ = 10 trials, with 20 cargos measured in each trial. Two-sample Welch's $t$ tests returned one significant $P$-value. *Bottom*: $n$ = 66 to 191 motile runs. Run-length distributions are provided in *SI Appendix*, Fig. S3.

membrane fluidity and motor diffusion by ~threefold (24, 27, 29) without microdomain formation (42). The concentration of nickel-loaded chelator lipid was kept constant for identical Kif5A attachment across cholesterol levels (Table 1) and membrane-enclosed cargos were blocked using incubation with excess casein to prevent nonspecific motor attachment (*Materials and Methods*). In addition to the in vivo scenario of ~1 to 2 kinesin per cargo examined in Fig. 1, we assayed a higher motor number range that is anticipated (37) to increase the sensitivity of cargo run length to changes in the binding rate of the motor; a higher motor number range may also be relevant for long-range transport in vivo (24).

For cargos carried by ~1 to 2 kinesins, adding cholesterol to the DOPC bilayer amplified the inhibitory effect of tau on motile fraction but not on run length (Fig. 2*A*). Here we employed the same Kif5A concentration as in Fig. 1*B*. In the absence of tau, the fraction of motile cargos remained constant at ~75% irrespective of membrane cholesterol; the mean run lengths of these motile cargos also remained unaffected (Fig. 2*A*). Motile fraction in the absence of tau reflects the probability of there being at least one active kinesin attached to the cargo (*Materials and Methods*; and refs. 6, 32, and 34). The null effect of cholesterol (Fig. 2*A*, *Top*) therefore indicates that kinesin attachment to cargos was unchanged across cholesterol levels, and that cholesterol addition did not significantly disrupt the cargo membrane. In the presence of tau, the fraction of motile cargos declined ~twofold further as membrane cholesterol increased to 50 mol% (Fig. 2*A*, *Top*); however, there was no further decrease in run length over this range of increasing cholesterol concentrations (Fig. 2*A*, *Bottom* and *SI Appendix*, Fig. S5). These results recapitulate our data comparing membrane-enclosed cargos with membrane-free cargos at the same Kif5A concentration (Fig. 1*B*), suggesting that changes in kinesin diffusion underlie both sets of observations. The significant effect of cholesterol on motile fraction (Fig. 2*A*, *Top*) indicates that cholesterol amplifies the inhibitory effect of tau on the binding rate of kinesin. The null effect of cholesterol on run length (Fig. 2*A*, *Bottom*) on the other hand indicates that the run length in these experiments is minimally impacted by changes in binding rate. Furthermore, under conditions for which the cargo run length is insensitive to binding rate, current descriptions indicate that the run length of the cargo is primarily determined by the unbinding rate of the single motor (37, 38). Our run-length data here (Fig. 2*A*, *Bottom*) thus indicate that increases in membrane cholesterol do not significantly impact the unbinding rate of Kif5A.

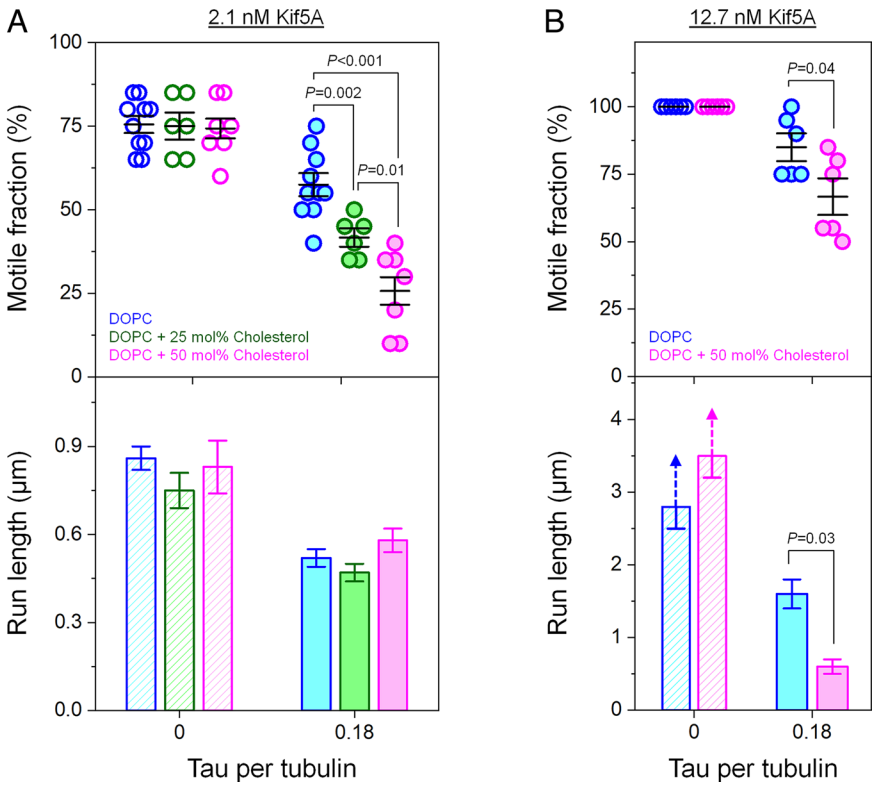


**Fig. 2.** Membrane cholesterol amplifies the inhibitory effect of tau on kinesin-1. (*A*) Transport of membrane-enclosed cargos in the physiological range of ~1 to 2 kinesins per cargo (as in Fig. 1*B*) in the absence and presence of tau, for three cholesterol levels (blue: 0 mol%; green: 25 mol%; magenta: 50 mol%). The concentration of Kif5A was kept constant at 2.1 nM. *Top*: Motile fraction of cargos. Horizontal lines indicate mean and 68% CI. $n$ = 6 to 10 trials, with 20 cargos per trial. Significant $P$-values from two-sample Welch's $t$ tests are indicated. *Bottom*: Mean run length of motile cargos. Error bars indicate SEM. $n$ = 21 to 113 motile runs. Run-length distributions and representative movies of cargo motility are provided in *SI Appendix*, Fig. S5 and Movies S2–S7. (*B*) Transport of membrane-enclosed cargos at a higher motor number range (~4 or more kinesins per cargo) in the absence and presence of tau, for two cholesterol levels (blue: 0 mol%; magenta: 50 mol%). The concentration of Kif5A was kept constant at 12.7 nM. CIs and error bars are as described in (*A*). *Top*: $n$ = 10 trials, with 20 cargos per trial. Two-sample Welch's $t$ tests indicated one significant $P$-value. *Bottomn* = 52 to 116 motile runs. Mann–Whitney $U$ tests returned one significant $P$-value. Dashed arrows indicate that the mean run lengths are lower bound estimates, given that a substantial fraction of cargos exceeded the 8-μm field of view. Run-length distributions and representative movies of cargo motility are provided in *SI Appendix*, Fig. S6 and Movies S8–S11.

For cargos carried by substantially more motors, membrane cholesterol amplified the inhibitory effect of tau on run length as well as on motile fraction (Fig. 2*B*). Here we increased the Kif5A concentration by ~sixfold from that in Fig. 2*A*, resulting in tau-free run lengths >fourfold longer than that of cargos carried by a single Kif5A (*SI Appendix*, Fig. S6). The extended run lengths indicate that the cargos were carried by ~four or more kinesins, based on prior results relating run length to kinesin motor number (43–47). In the absence of tau, we again observed similar motile fractions and run lengths independent of membrane cholesterol (Fig. 2*B*). In the presence of tau, there was a further ~2.6-fold decrease in cargo run length as membrane cholesterol increased from 0 to 50 mol% (Fig. 2*B*, *Bottom* and *SI Appendix*, Fig. S6), in addition to a significant further decrease in motile fraction over the same cholesterol increase (Fig. 2*B*, *Top*). Note that, despite the increase in motor number, the run length of cargos along tau-decorated microtubules did not increase appreciably in experiments employing 50 mol% cholesterol (Fig. 2, *Bottom*). This result is consistent with the fact that the extent to which additional motors on the cargo can contribute to run length is limited by the motor's binding rate (37, 38). A similar effect was observed previously for membrane-free cargos (14, 28). These results again indicate that cholesterol reduces the binding rate of kinesin in the presence of tau; they also highlight the potential of membrane cholesterol in impacting cargo run length even in the absence of a substantial effect on the unbinding rate.

**Membrane Cholesterol Reduces Kinesin Binding to Microtubules in the Presence of Tau.** We next expanded our experiments in Fig. 2 to examine the detailed dependence of motile fraction on kinesin concentration in the absence of tau and in the presence of tau, and how these dependences are impacted by membrane cholesterol (Fig. 3*A*). We employed the same membrane-enclosed cargos and the same tau concentration as in Fig. 2, and we examined three additional Kif5A concentrations. At each Kif5A concentration tested, membrane cholesterol consistently amplified tau inhibition of motile fraction (filled circles, Fig. 3*A*) but did not impact motile fraction in the absence of tau (open circles, Fig. 3*A*). At higher cholesterol levels, higher concentrations of Kif5A were needed to obtain the same motile fraction on tau-decorated microtubules (Fig. 3*A*). The null effect of cholesterol in the absence of tau again confirms that kinesin attachment to cargos was identical across cholesterol levels, and that membrane cholesterol did not significantly disrupt the cargo membrane. The significant effect of cholesterol in the presence of tau demonstrates membrane cholesterol as a general and sensitive factor tuning the binding of kinesin-based cargos to tau-decorated microtubules and potentially the flux of these cargos in vivo.

We next derived an analytical model of motile fraction to provide quantitative measures of kinesin binding in the presence of tau. Because we used the same preparation of kinesin–cargo complexes to compare transport on tau-free and tau-decorated microtubules (*Materials and Methods*), reduction in motile fraction in the presence of tau indicates reduction in the probability

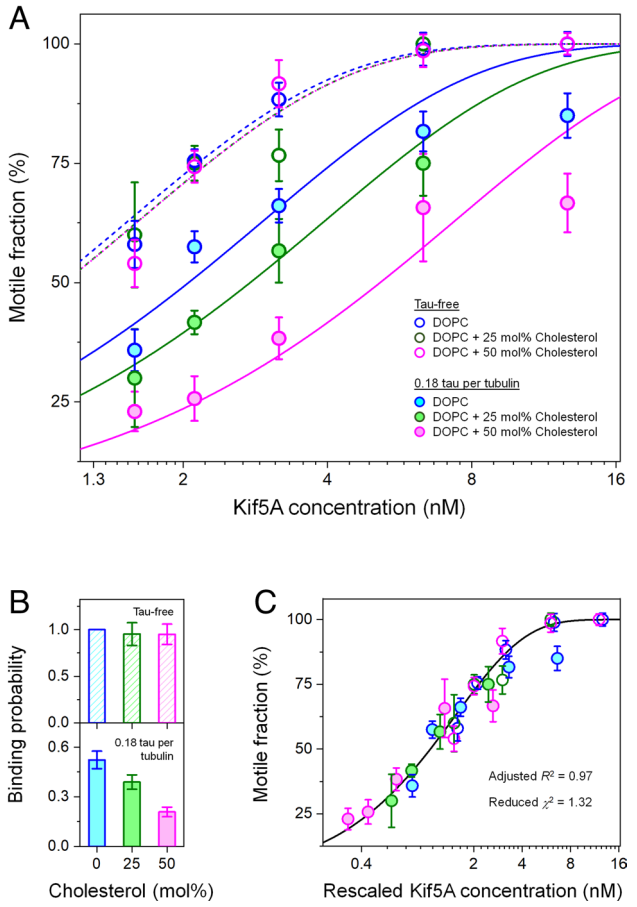


**Fig. 3.** Membrane cholesterol reduces kinesin binding to microtubules in the presence of tau. (*A*) Motile fraction of membrane-enclosed cargos as a function of Kif5A concentration in the absence and presence of tau, for three cholesterol levels (blue: 0 mol%; green: 25 mol%; magenta: 50 mol%). Dashed and solid lines indicate best fits to our analytical model of motile fraction (Eq. 1) with fitting parameter $\alpha$ shared among all six datasets; and binding probability $p$ constrained as one for tau-free data with 0 mol% cholesterol and determined separately for the remaining five datasets. Dashed lines indicate best fits to data from tau-free conditions; solid lines indicate best fits to data measured in the presence of tau; reduced $\chi^2$ = 1.63 and adjusted $R^2$ = 0.96. Error bars indicate SEM. $n$ = 2 to 10 trials, with 20 cargos measured for each trial. Individual trials at 2.1 nM and 12.7 nM Kif5A are shown in Fig. 2. (*B*) Microtubule-binding probability of Kif5A as a function of cholesterol levels, determined via the best-fits in (*A*). Error bars indicate the SE of the fit. (*C*) Multiplying Kif5A concentration by the best-fit binding probabilities ("Rescaled Kif5A concentration") collapsed all datasets from (*A*) onto a single master curve. Motile fraction measurements, sample sizes, and error bars are as indicated in (*A*); best-fit binding probabilities are as indicated in (*B*). Solid line indicates the previous model of motile fraction (6, 32) that assumes a binding probability of one. Two measures of goodness of fit are indicated.

that an active kinesin on the cargo binds the microtubule. Such reduction in binding probability, however, is not considered in the previous description of motile fraction (6, 32), which assumes that each motor binds to the microtubule with a probability of one. Here we extended the analytical description of motile fraction to consider binding probabilities below one. As in the previous derivation (6, 32), we considered the experimental scenario in which the number of motors on the cargo is Poisson-distributed. We then modeled motile fraction as the probability that each cargo is carried by at least one motor protein, multiplied by the probability that at least one of these motor proteins binds the microtubule, summed over all cargos in a population. Under the assumption that each motor binds the microtubule identically and independently, we have (*SI Appendix*, *Note 1*)

$$\text{Motile fraction} = 1 - e^{-p\alpha[M]} \quad [1]$$

where $0 \le p \le 1$ is the probability that a single motor binds the microtubule within the interaction time (30 s; Fig. 1*A*, *Inset*), and $\alpha$ is a fitting parameter relating the number of motors bound to the cargo to $[M]$, the concentration of motors used to prepare the motor–cargo complex. For a binding probability of one, our model returns $1 - e^{-\alpha[M]}$, the same expression as that previously developed (6, 32). As the binding probability decreases below one, our model predicts that the fundamental dependence of motile fraction on motor concentration remains unchanged, whereas the motor concentration is effectively rescaled by the binding probability $p$. This prediction is supported by our experimental finding that higher concentrations of Kif5A were needed at higher cholesterol levels to obtain the same motile fraction in the presence of tau (Fig. 3*A*).

Our model in Eq. 1 accurately captures our motile-fraction measurements (reduced $\chi^2$ = 1.63 and adjusted $R^2$ = 0.96; Fig. 3*A*). Because we employed the same motor-attachment strategy across experiments (Table 1), the fitting parameter $\alpha$ in Eq. 1 was shared among datasets. Additionally, kinesin was also previously shown to have a unit probability of binding to tau-free microtubules within the interaction time of 30 s (14, 32, 33). We therefore constrained the binding probability for one set of the tau-free data (0 mol% cholesterol) to be one and examined how the binding probability is impacted by changes in tau concentration or cholesterol levels. In the absence of tau, adding cholesterol to the cargo membrane did not significantly impact the binding probability of kinesin, which remained one within fitting uncertainty (Fig. 3*B*, *Top*). In the presence of tau, the best fits returned binding probabilities below 1 (Fig. 3*B*, *Bottom*); there was a ~2.5-fold further reduction in binding probability as membrane cholesterol increased from 0 mol% to 50 mol% (Fig. 3*B*, *Bottom*). Underscoring the goodness of this global fit, rescaling motor concentrations by best-fit binding probabilities (Fig. 3*B*) collapsed all six sets of motile-fraction measurements onto a single master curve (reduced $\chi^2$ = 1.32 and adjusted $R^2$ = 0.97; Fig. 3*C*). These results indicate that the fundamental mechanism underlying motile probability is not impacted by tau or membrane cholesterol. Instead, reduction of motile fraction by tau and membrane cholesterol may be understood as effectively rescaling the kinesin concentration by the binding probability of the motor. Tau reduces this binding probability; membrane cholesterol amplifies tau inhibition, further reducing kinesin-binding probability in the presence of tau (Fig. 3*B*, *Bottom*).

**Proposed Mechanism Linking Motor Diffusion to Kinesin Binding in the Presence of Tau.** Thus far, our experimental and theoretical investigations (Figs. 2 and 3; and Eq. 1) demonstrate that membrane cholesterol reduces the probability that kinesin on the cargo binds the microtubule in the presence of tau (Fig. 3*B*, *Bottom*). Because we measured motile fractions over the same 30-s duration (Fig. 1*A*, *Inset*), reduction in binding probability indicates reduction in the rate at which the motor binds the microtubule.

The kinesin–microtubule interaction is short-ranged, and the term microtubule-binding rate can be ambiguous without considering experimental geometry. In this study, binding rate is defined as that of a kinesin in complex with a cargo that is held near a microtubule (Fig. 1*A*, *Inset*). This definition of binding rate is common in the literature, including studies that established the binding rate of kinesin in the absence of tau (48) and the inhibitory effect of tau on kinesin binding (14). Note that our cargo size exceeds the extension length of kinesin (49, 50), thus the motor must first reach the microtubule before it can interact

locally with open tubulin dimers for binding. Although changes in kinesin diffusion in the cargo membrane may impact how fast the motor can reach the microtubule, our tau-free data indicate that the motor reached the microtubule within our experimental duration irrespective of cholesterol level (binding probability = 1, Fig. 3*B*, *Top*). We therefore deduce that, in the presence of tau, the main effect of cholesterol occurred after the motor has reached the microtubule.

We propose that cholesterol amplifies tau inhibition by prolonging the diffusive search time for open binding sites on the microtubule. To explore this proposed mechanism, we developed a simple one-dimensional model in which a motor diffusively searches for open binding sites on the microtubule (Fig. 4*A*). We assumed that open binding sites are separated by a characteristic distance $\Delta x$. We further assumed that kinesin binds each open binding site identically. Each time the motor encounters an open binding site, there is a likelihood $\eta$ that the motor binds. If the motor does not bind at an encounter, then the motor diffuses to the nearest open site where it again has a likelihood $\eta$ to bind. Under these simplifying assumptions, the rate that the motor encounters an open binding site is $D/\Delta x^2$ (*SI Appendix*, *Note 2*), the rate that the motor binds an open binding site is $D\eta/\Delta x^2$, and the probability that the motor binds the microtubule within interaction time $T$ is

$$\text{Binding Probability} \;=\; 1 - e^{-D\eta T/\Delta x^2} \qquad [2]$$

where $D$ is the diffusion constant of the motor in the cargo membrane.

Eq. **2** provides a simple conceptual framework to explore the proposed mechanistic link between motor diffusion, tau, and kinesin binding. For a given diffusion constant, Eq. **2** predicts that the binding probability of the motor decreases as the characteristic distance between open binding sites increases. This general prediction agrees well with our experiments employing increasing concentrations of tau (for example, membrane-enclosed cargo in Fig. 1*A*, *Top*), indicating that increases in binding-site distance capture the key effect of tau in our experiments. Note that, whereas $\Delta x$ may be reasonably estimated by the 8-nm tubulin spacing on tau-free microtubules (51), its value in the presence of tau is less easily determined. The inhibitory effect of tau on kinesin binding is significantly greater than what might be naively expected from the tau:tubulin incubation ratio (14, 15). Recent studies demonstrate that tau is not statically bound but instead diffuses on the microtubule (11, 12, 52, 53), which may increase its steric inhibition of binding sites well-above its incubation stoichiometry. Furthermore, because the motor diffusion occurs on a two-dimensional cargo surface, the motor can diffuse away from (and back into) the microtubule neighborhood as it searches for an open binding site. Such excursions would increase $\Delta x$ in Eq. **2** above the linear distance between open binding sites on the microtubule. The frequency of such excursions is likely negligible in the absence of tau but increases as the number of open binding sites on the microtubule decreases. Given these considerations, we made no a priori assumption about $\Delta x$ in the presence of tau. Instead, we determined this parameter via the least-square fitting of our model (Eq. **2**) to our experimental findings employing tau-decorated microtubules (Fig. 3*B*).

We estimated the diffusion constant $D$ and the intrinsic binding likelihood $\eta$ in Eq. **2** based on well-established literature values. The fitted value of $\Delta x$ in the presence of tau scales as the square root of the two estimated parameters (diffusion constant $D$ and intrinsic binding likelihood $\eta$) and therefore has limited sensitivity to potential differences between their experimental and estimated values. For the diffusion constant $D$, we used the published values of kinesin diffusion in planar-supported DOPC membranes containing a similar range of membrane cholesterol (29) as a starting point, and reduced these values by 2.6-fold to account for the additional frictional drag (54) associated with the nickel–hexahistidine interaction in our Kif5A-membrane attachment strategy in accordance with previous results (55). We therefore estimated diffusion constants of 0.5, 0.3, and 0.2 $\mu m^2/s$ for Kif5A attached to DOPC membranes containing 0, 25, and 50 mol% cholesterol, respectively. Note that, direct measurements of motor diffusion have not yet been realized for our cargo size (0.5-μm diameter); for larger, 5-μm-diameter cargos, recent super-resolution stimulated emission depletion fluorescence correlation spectroscopy (STED-FCS) measurements demonstrate similar lipid diffusivity (at 0 and 50 mol% cholesterol) for membrane-enclosed cargos and planar-supported membranes (27). To estimate the binding likelihood $\eta$ at each encounter, we combined our model for the binding rate of the motor ($D\eta/\Delta x^2$) with a previous study that reported both the binding rate ($4.7 \pm 2.4\ s^{-1}$) and the diffusion constant ($1 \pm 0.5\ \mu m^2/s$) of a membrane-bound kinesin in the absence of tau (48). Using an estimated value $\Delta x = 8$ nm for tau-free microtubules (51), we estimated $\eta = (3 \pm 2) \times 10^{-4}$ as the intrinsic likelihood that kinesin binds an open binding site at each encounter. Under the assumption that neither cholesterol nor tau influences the intrinsic binding likelihood $\eta$, we evaluated the predicted binding probability within our experimental duration ($T = 30$ s) and for a range of binding-site distances ≥8 nm (Fig. 4*B*).

Our simple model in Eq. **2** captures the key observations in our experiments (Fig. 4 *B*–*D*). At a characteristic distance of 8 nm, which reflects the tau-free condition, Eq. **2** predicts a binding probability of one for all three diffusion constants (Fig. 4*B*), in good agreement with our experimental finding that membrane cholesterol does not impact kinesin-microtubule binding in the absence of tau (Fig. 4*C*, *Top*). As the binding-site distance increased, the binding probability reduced; this reduction was amplified as the motor diffusion decreased (Fig. 4*B*). Least-square fitting of the predictions of Eq. **2** to our experimental data in Fig. 3*B* yielded an effective binding-site distance of ~78 ± 26 nm in the presence of tau (vertical dashed line, Fig. 4*B*), capturing both the overall reduction in binding probability from the tau-free condition and the ~twofold further reduction in binding probability at higher cholesterol levels (Fig. 4*C*, *Bottom*). This effective distance likely reflects the known super-stoichiometric tau inhibition (14, 15) and may include two-dimensional excursions of the motor on the cargo surface as the motor searches for an open binding site, both of which would increase $\Delta x$ estimated in the model. Combining the predicted binding probabilities with our description of motile fraction in Eq. **1**, we recapitulate the effects of cholesterol on motile fraction (Fig. 4*D*). Taken together, our simple model supports our proposed mechanism and identifies diffusion of individual motors in the cargo membrane as a rate-limiting step in kinesin binding to microtubules in the presence of tau.

## Discussion

Intracellular cargos are often membrane-bound and transported by microtubule-based motors in the presence of MAPs. Here, we established a direct link between the physical properties of the cargo membrane and MAP-based regulation of a major microtubule-based motor kinesin-1. Attaching kinesins to a fluid lipid membrane decreased the inhibitory effect of tau in comparison to membrane-free cargos, under conditions in which the two classes of cargos exhibit the same motile fraction in the absence

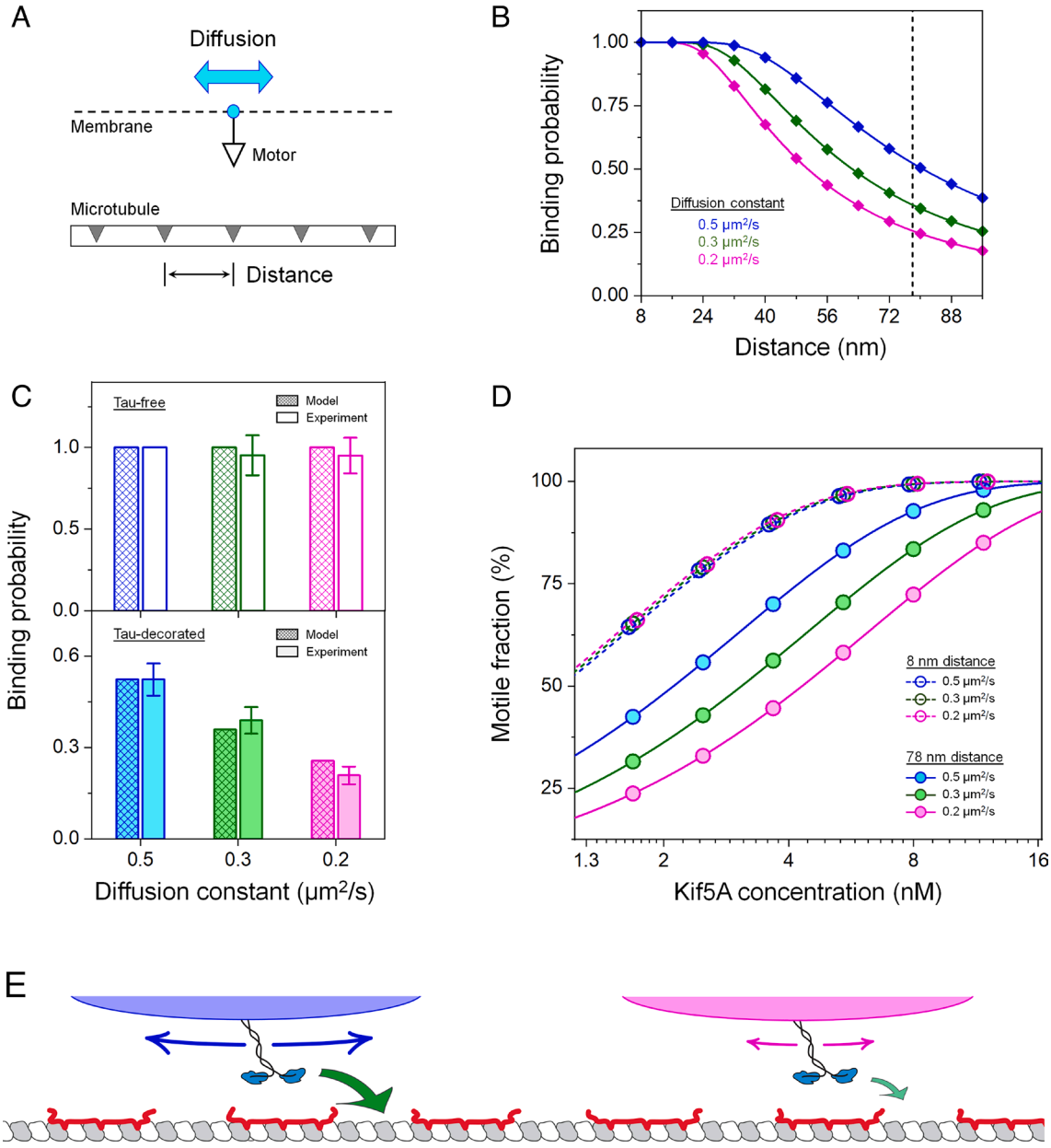


**Fig. 4.** A mechanistic model linking motor diffusion to kinesin binding in the presence of tau. (*A*) Schematic of the model: A membrane-bound motor diffusively searches for open binding sites (shaded regions) on the microtubule. The motor and microtubule are vertically offset for visualization. The effect of tau is modeled as an increase in the characteristic distance between open binding sites on the microtubule. The effect of membrane cholesterol is modeled as a decrease in the diffusion constant of the motor in the cargo membrane. The analytical form of this one-dimensional model is shown in Eq. **2**. (*B*) Model predictions of the probability that a kinesin binds a microtubule within the interaction time of 30 s, for motor diffusion constants that approximate the effects of cholesterol in our experiments (blue: 0.5 $\mu m^2/s$; green: 0.3 $\mu m^2/s$; magenta: 0.2 $\mu m^2/s$). Vertical dashed line, characteristic binding-site distance in the presence of tau (78 nm), determined via least-square fitting of predictions of Eq. **2** to experiments employing tau-decorated microtubules (Fig. 3*B*). (*C*) Comparison of model predictions and experimental values of the microtubule-binding probability for a single kinesin. Model predictions are as determined in (*B*) for the characteristic distances of 8 nm (*Top*) and 78 nm (determined via least-square fitting of predictions in *B* to experiments in Fig. 3*B*) (*Bottom*). Experimental values are as determined in Fig. 3*B* for 0 mol % cholesterol (blue), 25 mol % cholesterol (green), and 50 mol % cholesterol (magenta). (*D*) Motile fraction calculated based on Eq. **1**, using binding probabilities predicted in (*C*) and the fitting parameter $\alpha$ determined in Fig. 3*A*. Motile fractions for a characteristic distance of 8 nm (dashed lines and open symbols) are laterally offset for visualization. (*E*) Proposed mechanism: reduction in kinesin diffusion in the cargo membrane underlies the effect of cholesterol on kinesin binding in the presence of tau.

of tau (Fig. 1). Adding cholesterol to the cargo membrane increased the inhibitory effect of tau in a dosage-dependent manner (Figs. 2 and 3). These results reveal the potential of cargo membrane properties to regulate kinesin-based transport in vivo, for example under tau-enriched conditions such as those found in neurons, and/or in combination with factors (36, 56, 57) that alter tau binding to the microtubule.

We found that increasing the cholesterol level in the cargo membrane decreases the rate that kinesin binds microtubules in the presence of tau (Fig. 3*B*; and Eq. **1**). Cholesterol is increasingly linked to cargo transport in vivo (19, 58, 59). The level of membrane-associated cholesterol in intracellular cargos can vary as part of the maturation process (19) or disease pathology (58, 59). Recent investigations have found that cholesterol-rich microdomains promote clustering of cytoplasmic dynein (19) and a monomeric kinesin (60) on the cargo membrane; such a clustering effect was not observed for the dimeric kinesin-1 (19). Here, we employed levels of cholesterol within its solubility limit [~67

mol% in DOPC, references (41, 42)], reducing membrane fluidity and motor diffusion (24, 27, 29) without microdomain formation (42). Our findings therefore identify a mechanism through which cholesterol can impact motor protein-based transport, which may be important for tuning motility without changing the number of kinesins carrying the cargo, for example in neuronal transport of cargos driven by a stable assembly of kinesins (17, 61).

We propose that reduction in kinesin diffusion in the cargo membrane underlies the effect of cholesterol on kinesin binding in the presence of tau (Fig. 4*E*). Our model in Eq. **2** provides a simple conceptual framework to explore this proposed mechanism. The model is akin to the collision theory of chemical reactions, which describes reaction rate as the product of the frequency of collision between reactants and the likelihood that each collision results in a reaction. Here we examined the binding rate between two reactants: the open binding sites on the microtubule and the individual kinesin molecule that diffuses in the cargo membrane. Tau reduces the frequency of collision between reactants by reducing the concentration of one reactant (the open binding sites), whereas motor diffusion tunes the time that it takes for one reactant (the unbound motor) to encounter the other reactant (the open binding sites) via diffusive search. An increase in motor diffusion constant decreases the diffusive search time for open binding sites and reduces inhibition by tau, whereas a decrease in motor diffusion constant increases the diffusive search time and amplifies inhibition by tau. In vivo, these membrane-based changes in binding rate may impact motile probability at lower tau concentrations, as the cargo likely has a shorter time to bind than in our experiments (30 s; Fig. 1*A*, *Inset*). Note that, tau may reduce kinesin binding by increasing the characteristic distance between open binding sites ($\Delta x$) and/or by reducing the intrinsic binding interaction between kinesin and open binding sites ($\eta$ in Eq. **2**). Here we modeled tau inhibition as an increase in $\Delta x$ (Fig. 4 *B*–*D*); the proposed mechanism would also hold true if we modeled tau inhibition as a reduction in $\eta$ or a combination of both parameters. Future investigations clarifying the mechanism underlying the super-stoichiometric inhibition by tau will help disentangle the relative contributions of these two potential mechanisms of tau inhibition.

By necessity, our simple model in Eq. **2** does not capture the full range of molecular details present in our experimental system. For example, we examined motor diffusion in one dimension, whereas the actual diffusion process occurs on the two-dimensional cargo surface. We also did not include details related to the distribution or the dynamics of tau on the microtubule (11, 12, 52, 53), or how far the motor can extend to reach the microtubule at the cargo-microtubule interface (34, 62). Additionally, as the distance between binding sites and thus the diffusive search time decreases, molecular interactions between kinesin and individual binding sites (63–65) likely become rate-limiting for kinesin binding to the microtubule (as indicated by our tau-free data, Figs. 1–3; and refs. 23 and 24). Further work integrating these molecular details, combined with experimental realization of diffusion measurements on submicron-sized cargos and mechanistic understanding of how tau reduces kinesin binding to the microtubule, will help extend the model that we developed here to refine the mechanism underlying the kinesin–microtubule binding process.

The effects of membrane cholesterol may more broadly extend to other lipid alterations that impact motor diffusion in the cargo membrane, including those associated with aging and neurological diseases (20, 21). Similarly, factors other than MAP tau can occlude kinesin binding on the microtubule (13, 66–68). Our analytical expression of motile fraction (Eq. **1**) extends a previous model (6, 32) and may be generally applied to probe reduced motor binding in standard optical trapping assays. We anticipate that diffusion of individual motors in the cargo membrane may constitute a general mechanism influencing binding to the microtubule, and we speculate that age-related changes in lipid membranes might help explain why some inherited mutations in kinesins result in delayed onset diseases [such as those caused by Kif5A (3–5)]. Conversely, our work suggests the possibility of targeting membrane fluidity to overcome transport dysfunctions that are a common early hallmark of aging and neurological diseases (22). Finally, extensive investigations have identified physiological factors that affect binding interactions between kinesin and tubulin, including MAPs (9, 69–71) and posttranslational modifications of tubulin (72–75). The work presented here provides a general framework for future studies examining the interplay between these factors and cargo membrane properties and how they contribute to the rich regulation of kinesin-based transport in vivo.

## Materials and Methods

**Materials.** Human kinesin-1 heavy chain isoform Kif5A (full-length) with a C-terminal hexahistidine tag was expressed in *Escherichia coli* BL21(DE3) cells and purified as described (76); the final construct was a Kif5A homodimer with two C-terminal hexahistidine tags. Human kinesin-1 heavy chain isoform Kif5B consisting of residues 1 to 560 with a C-terminal Halo tag was expressed in *Escherichia coli* BL21(DE3) cells and purified as described (23). The purified Kif5B protein was incubated with 10 μM HaloTag PEG-Biotin ligand (Promega) for 30 min on ice to produce a final construct of Kif5B homodimer with two C-terminal biotin tags. Unbound ligand was removed via dialysis and buffer was exchanged using 3,000 Da dialysis membrane (Fisher). Human tau isoform encoding 352 amino acids with three microtubule-binding repeats (hTau23, or 3RS tau) was expressed in *Escherichia coli* and purified as described (14). Tubulin was purified from bovine brain via two cycles of polymerization and depolymerization and phosphocellulose chromatography as described (14). All proteins (Kif5A, Kif5B, tau, and tubulin) were flash-frozen and stored at −80 °C until use. Representative SDS–PAGE gels of purified proteins are provided in *SI Appendix*, Fig. S7. Lipids 18:1 (Δ9-Cis) PC (DOPC), 18:1 DGS-NTA(Ni), and DSPE-PEG(2000) Biotin were purchased from Avanti Polar Lipids. Cholesterol ($C_{27}H_{46}O$) was purchased from Sigma-Aldrich. Streptavidin was purchased from Thermo Fisher. Chemicals were purchased from Sigma-Aldrich. Silica microspheres (0.5 μm in diameter; 10.2% solids) were purchased from Bangs Laboratories. Carboxylated polystyrene microspheres (0.5 μm in diameter; 2.5% solids) were purchased from Polysciences.

**Membrane-Enclosed Cargo Preparation.** Membrane-enclosed cargos were prepared via vesicle fusion using lipid mixtures containing 0 mol% cholesterol (23, 25–27) and lipid mixtures containing up to 50 mol% cholesterol (27). Briefly, lipid mixtures (Table 1) were dried under vacuum at room temperature overnight, resuspended to 4 mM in HNa100 buffer (pH 7.0, 20 mM HEPES, 100 mM NaCl, 1 mM EGTA, 1 mM dithiothreitol) via five freeze–thaw cycles, and passed through a 30-nm polycarbonate membrane 21 times using a mini-extruder (Avanti Polar Lipids) to generate small unilamellar vesicles. Silica microspheres (40 μL stock) were bath-sonicated in 1 mL methanol for 1 min, resuspended in 1 mL 1 N KOH and bath-sonicated in ice water for 10 min, washed seven times in 1 mL Nanopure water, and resuspended in 40 μL Nanopure water. Freshly washed silica beads (9 μL) were incubated with 150 μL 2 mM freshly extruded small unilamellar vesicles for 30 min at room temperature, washed four times in 1 mL HNa100, resuspended in 100 μL 5.55 mg/mL casein solution in PMEE buffer (35 mM PIPES, 5 mM $MgSO_4$, 1 mM EGTA, 0.5 mM EDTA, pH 7.1) for blocking at room temperature for 30 min. Note that, as a blocking protein, casein can serve two roles in motility assays. When not in excess, casein can reduce the likelihood of kinesin denaturing on a glass surface (77) and reduce the likelihood of kinesin binding the glass surface via its motor domain (78). Blocking with excess casein as employed here (25), however, prevents nonspecific adsorption of proteins including kinesin on glass surfaces (13, 14, 25). For preparations using lipid mixtures containing a nickel-loaded chelator lipid (Membranes *B*–*D*, Table 1), the resulting membrane-enclosed cargos were kept at 4 °C for use within 2 d. For preparations using a lipid mixture containing a biotinylated lipid (Membrane *A*, Table 1), the membrane-enclosed cargos were washed three times in 1 mL HNa100, resuspended in 40 μL 1 mg/mL streptavidin at room temperature for

1 h, washed three times in 1 mL HNa100, resuspended in 100 μL HNa100, and kept at 4 °C for use within 2 d.

**Lipid Vesicle Preparation.** A cholesterol-free DOPC lipid mixture (Membrane *B*, Table 1) was dried under vacuum and resuspended in HNa100 as described above for membrane-enclosed cargos. The lipid mixture was then extruded through a 100-nm polycarbonate membrane 21 times using a mini-extruder (Avanti Polar Lipids). Lipid vesicles were used immediately following extrusion.

**Kinesin–Cargo Complex Preparation.** Kif5A was attached to membrane-enclosed cargos via a nickel–hexahistidine interaction (23, 30); cargo-mediated activation was previously demonstrated for full-length Kif5A (76). Kif5B was attached to membrane-enclosed cargos via a streptavidin–biotin interaction (24, 26, 30). Both kinesin isoforms were attached to membrane-free polystyrene microspheres via nonspecific interactions (23, 33, 34). Kinesin motors were incubated with membrane-enclosed cargos or membrane-free cargos in motility buffer (67 mM PIPES, 50 mM $CH_3CO_2K$, 3 mM $MgSO_4$, 1 mM dithiothreitol, 0.84 mM EGTA, 10 μM taxol, pH 6.9) for 10 min at room temperature. The solution was then supplemented with an oxygen-scavenging solution (250 μg/mL glucose oxidase, 30 μg/mL catalase, 4.6 mg/mL glucose) and 1 mM ATP, followed by immediate use for optical trapping experiments.

The concentration of membrane-free cargos was kept constant at 0.6 pM, and the concentration of membrane-enclosed cargos was kept constant at 0.55 pM. These concentrations were empirically determined to optimize the number of cargos in the field of view for optical trapping.

The concentration of kinesin in each experiment was empirically tuned to obtain the indicated motile fraction on tau-free microtubules. In each kinesin–cargo mixture, the number of active kinesins attached to each cargo is Poisson-distributed and a substantial fraction of the cargo can have no active kinesin attached. The probability that the cargo has at least one motor is $1 - e^{-m}$, where $m$ is the mean number of active motors attached to each cargo (6, 32). In the absence of tau, our experimental duration of 30 s (Fig. 1*A*, *Inset*) is sufficient for binding if there is a single active kinesin on the cargo (6, 32, 33). The resulting motile fraction measurement therefore directly indicates the probability that a cargo is carried by at least one active kinesin (6, 32). Moreover, for the 0.5-μm diameter cargos used in this study, the fraction of motile cargos being carried by two or more active kinesins has been characterized for motile fractions ranging between 15 and 85% in the absence of tau (34). Note that the incubation ratio of kinesin to cargos does not equate the mean number of active kinesins attached to the cargo. Three factors are known to limit the number of active kinesins per cargo well below their incubation ratio: 1) not all kinesins in solution can bind the cargo, 2) not all kinesins bound to the cargo are active, and 3) not all active kinesins on the cargo can reach the microtubule at the same time. Importantly, it is currently not possible to estimate the percentage of auto-inhibited cargo-bound motors, given that the nature and the impact of the activation mechanisms for kinesin-1 are still under active investigation (9, 33, 69–71).

For measurements in Figs. 1 and 2*A*, the concentrations of kinesins were tuned to obtain a motile fraction of ~75% on tau-free microtubules, corresponding to ~30% of motile cargos being carried by two or more active kinesins (34) and mimicking the in vivo scenario (17–19). In Fig. 1*A*, the concentration of Kif5B was kept constant at 1.7 nM in experiments employing membrane-free cargo and 4.5 nM in experiments employing membrane-enclosed cargos. The higher Kif5B concentration used for membrane-enclosed cargos likely reflects the fact that the number of specific attachment sites for kinesin in the lipid membrane is lower than that of the nonspecific attachment sites in the membrane-free case. In Fig. 1*B*, the concentration of Kif5A was kept constant 3.8 nM in experiments employing membrane-free cargos and 2.1 nM in experiments employing membrane-enclosed cargos. The lower Kif5A concentration used for membrane-enclosed cargos likely reflects the fact that cargo-mediated activation of the full-length kinesin requires specific binding of the kinesin tail domain to the cargo (79, 80), which is satisfied via specific attachment to membrane-enclosed cargos but not necessarily satisfied via the nonspecific attachment to membrane-free cargos. Whereas more kinesins can in principle attach to membrane-free cargos nonspecifically, this attachment is not necessarily via the motor's tail domain and may not relieve the tail-dependent autoinhibition on the full-length kinesin attached to the cargo. In Fig. 2*A*, the concentration of Kif5A was kept constant at 2.1 nM across cholesterol levels.

For measurements in Figs. 2 *B* and 3 *A*, the concentrations of Kif5A were tuned to achieve a motile fraction range of ~55 to 100% on tau-free microtubules, encompassing the physiological range of ~1 to 2 kinesins per cargo (6, 32, 34) up to ~four or more kinesins per cargo (*SI Appendix*, Fig. S6; and refs. 43–47). The concentrations of Kif5A were kept constant at 2.1 nM in Fig. 2*A*, 12.7 nM in Fig. 2*B*, and between 1.6 and 12.7 nM as indicated in Fig. 3*A*. Each Kif5A concentration was kept constant across cholesterol levels. The lowest Kif5A concentration in these experiments (1.6 nM, Fig. 3*A*) yielded a motile fraction of ~55% on tau-free microtubules, corresponding to ~15% of motile cargos being carried by two or more active kinesins (34).

**Microtubule Preparation.** Tubulin (40 $\mu$M) was incubated in PM buffer (100 mM PIPES, 1 mM $MgSO_4$, 2 mM EGTA, pH 6.9) supplemented with 1 mM GTP for 20 min at 37 °C. The assembled microtubules were incubated with an equal volume of PM buffer supplemented with 40 $\mu$M taxol and 1 mM GTP for 20 min at 37 °C. Taxol-stabilized microtubules were diluted to 500 nM in microtubule buffer (PMEE buffer supplemented with 10 μM taxol and 1 mM GTP) and incubated with 0 to 130 nM hTau23 in microtubule buffer for 20 min at 37 °C, followed by immediate use for flow cell preparation. The concentration of tau in each microtubule preparation is represented as the incubation ratio of tau molecules per tubulin dimer. Tau coverage on microtubules was verified via immunostaining (81, 82) with an antibody against the N-terminal region of tau, or an antibody against the mid-domain of tau (*SI Appendix*, *Supplementary Methods* and Fig. S8). The inhibitory effect of tau on kinesin was verified by the decrease in motile fraction on tau-decorated microtubules. For each preparation, the inhibitory effect of tau on motile fraction remained constant (within measurement uncertainty) for the duration of each set of optical trapping experiments (up to ~5 h).

**Flow Cell Preparation.** Flow cells were constructed by sandwiching a cover glass and a microscope slide using double-sided tape. The cover glass was plasma cleaned and coated with poly-L-lysine for microtubule immobilization (66). Freshly prepared microtubules (tau-free or tau-decorated) were diluted to 45 nM in microtubule buffer and introduced into flow cells for incubation at room temperature for 10 min. The flow cell was then rinsed with microtubule buffer and then blocked with 5.55 mg/mL casein in microtubule buffer for 10 min at room temperature. In experiments in which the microtubules were incubated with excess DOPC lipid vesicles, flow cells were further incubated with 0 or 100 μM freshly extruded lipid vesicles in 5.55 mg/mL casein solution for 5 min at room temperature. The flow cells were then rinsed and blocked with 5.55 mg/mL casein in microtubule buffer for 10 min at room temperature. All flow cells were used within the same day of preparation.

**In Vitro Optical Trapping Experiments.** In vitro optical trapping experiments were carried out in flow cells at room temperature (23, 33, 34). Briefly, freshly prepared kinesin–cargo complexes were introduced to flow cells with immobilized microtubules. A cargo diameter of 0.5 μm was used, this cargo size is well suited for optical trapping and is in the range of vesicle sizes in vivo (17–19). A single-beam optical trap similar to that described previously (32) was used to position individual cargos near a microtubule. The trap power was limited to <20 mW at fiber output, such that the trap positioned individual cargos but did not stall cargos carried by a single kinesin. A motile event was scored if the cargo moved directionally away from the trap center within 30 s (14, 32, 33). The optical trap was then shut off to either release the unbound cargo or to measure cargo run length under zero external load. Cargo trajectories were imaged at 100× magnification via differential interference contrast microscopy and video-recorded using a Giga-E camera at 30 Hz. Each preparation of kinesin–cargo complexes was used to measure transport at two tau concentrations. Each preparation of microtubules was used to measure the transport of two or more cargo types. The measurement order of each experimental condition was shuffled to eliminate potential artifacts.

**Data Analysis.** Cargos were particle-tracked to 10-nm resolution (1/3 pixel) via a template-matching algorithm (83). The run length of each motile cargo was determined as the net displacement of the cargo along the microtubule between binding and unbinding. The distribution of run lengths for each experimental condition was fitted to a single exponential decay. To account for the time that elapsed before the manual shutoff of the optical trap, only runs >250 nm were analyzed. Runs that exceeded the experimental field of view were also excluded

from the fit. Mean run length and SEM for each distribution were determined as the fitted decay constant and uncertainty, respectively. Fitting the cumulative probability distribution of the run lengths, which does not require data binning, returned similar values of mean run lengths. The unbinding rate of the single kinesin (*SI Appendix*, Fig. S4) was determined as the ratio of the mean run length to the mean velocity of single-kinesin cargos; the associated SEM was determined via error propagation.

**Model Derivation.** Derivations of Eqs. **1** and **2** are detailed in *SI Appendix*, *Notes 1 and 2*.

**Statistical Analysis.** Two-sample Welch's *t* test was used to determine the statistical significance of differences between two distributions of motile-fraction measurements. The Mann–Whitney *U* test was used to determine the statistical significance of differences between two distributions of run-length measurements. The Kruskal–Wallis *H* test, a nonparametric ANOVA, was used to determine the statistical significance of differences between multiple distributions of run-length measurements.

**Data, Materials, and Software Availability.** All study data are included in the article and/or *SI Appendix*.

**ACKNOWLEDGMENTS.** This work was supported by the NIH (Grant Nos. R15 GM120682 to J.X. and R01 NS048501 to S.J.K.) and the NSF (Grant No. ENG-1563280 to M.V.). This work was supported in part by the intramural research program of the National Heart, Lung, and Blood Institute, NIH, Department of Human Services (ZIAHL001056 to K.C.N). We thank John A. Hammer, Serapion Pyrpassopoulos, Matthew J. Bovyn, Steven P. Gross, and Yasuharu Takagi for discussion. We thank Tiffany J. Vora (Bayana Science) and Yolanda L. Jones (NIH Library) for manuscript editing.

Author affiliations: [a]Department of Physics, University of California, Merced, CA 95343; [b]Laboratory of Single Molecule Biophysics, National Heart, Lung and Blood Institute, NIH, Bethesda, MD 20892; [c]Department of Physics, Oregon State University, Corvallis, OR 97331; [d]Department of Physics and Astronomy, University of Utah, Salt Lake City, UT 84112; and [e]Burnett School of Biomedical Sciences, University of Central Florida, Orlando, FL 32827

1. R. D. Vale, T. S. Reese, M. P. Sheetz, Identification of a novel force-generating protein, kinesin, involved in microtubule-based motility. *Cell* **42**, 39–50 (1985).
2. S. T. Brady, A novel brain ATPase with properties expected for the fast axonal transport motor. *Nature* **317**, 73–75 (1985).
3. E. Reid *et al.*, A kinesin heavy chain (KIF5A) mutation in hereditary spastic paraplegia (SPG10). *Am. J. Hum. Genet.* **71**, 1189–1194 (2002).
4. Y. T. Liu *et al.*, Extended phenotypic spectrum of KIF5A mutations: From spastic paraplegia to axonal neuropathy. *Neurology* **83**, 612–619 (2014).
5. A. Nicolas *et al.*, Genome-wide analyses identify KIF5A as a novel ALS gene. *Neuron* **97**, 1268–1283. e1266 (2018).
6. S. M. Block, L. S. Goldstein, B. J. Schnapp, Bead movement by single kinesin molecules studied with optical tweezers. *Nature* **348**, 348–352 (1990).
7. A. Yildiz, M. Tomishige, R. D. Vale, P. R. Selvin, Kinesin walks hand-over-hand. *Science* **303**, 676–678 (2004).
8. I. A. Telley, P. Bieling, T. Surrey, Obstacles on the microtubule reduce the processivity of kinesin-1 in a minimal in vitro system and in cell extract. *Biophys. J.* **96**, 3341–3353 (2009).
9. B. Y. Monroy *et al.*, A combinatorial MAP code dictates polarized microtubule transport. *Dev. Cell* **53**, 60–72.e64 (2020).
10. L. S. Ferro *et al.*, Structural and functional insight into regulation of kinesin-1 by microtubule-associated protein MAP7. *Science* **375**, 326–331 (2022).
11. R. Tan *et al.*, Microtubules gate tau condensation to spatially regulate microtubule functions. *Nat. Cell Biol.* **21**, 1078–1085 (2019).
12. V. Siahaan *et al.*, Kinetically distinct phases of tau on microtubules regulate kinesin motors and severing enzymes. *Nat. Cell Biol.* **21**, 1086–1092 (2019).
13. A. Seitz *et al.*, Single-molecule investigation of the interference between kinesin, tau and MAP2c. *EMBO J.* **21**, 4896–4905 (2002).
14. M. Vershinin, B. C. Carter, D. S. Razafsky, S. J. King, S. P. Gross, Multiple-motor based transport and its regulation by Tau. *Proc. Natl. Acad. Sci. U.S.A.* **104**, 87–92 (2007).
15. R. Dixit, J. L. Ross, Y. E. Goldman, E. L. Holzbaur, Differential regulation of dynein and kinesin motor proteins by tau. *Science* **319**, 1086–1089 (2008).
16. M. D. Weingarten, A. H. Lockwood, S. Y. Hwo, M. W. Kirschner, A protein factor essential for microtubule assembly. *Proc. Natl. Acad. Sci. U.S.A.* **72**, 1858–1862 (1975).
17. G. T. Shubeita *et al.*, Consequences of motor copy number on the intracellular transport of kinesin-1-driven lipid droplets. *Cell* **135**, 1098–1107 (2008).
18. A. G. Hendricks *et al.*, Motor coordination via a tug-of-war mechanism drives bidirectional vesicle transport. *Curr. Biol.* **20**, 697–702 (2010).
19. A. Rai *et al.*, Dynein clusters into lipid microdomains on phagosomes to drive rapid transport toward lysosomes. *Cell* **164**, 722–734 (2016).
20. M. Shinitzky, Patterns of lipid changes in membranes of the aged brain. *Gerontology* **33**, 149–154 (1987).
21. R. G. Cutler *et al.*, Involvement of oxidative stress-induced abnormalities in ceramide and cholesterol metabolism in brain aging and Alzheimer's disease. *Proc. Natl. Acad. Sci. U.S.A.* **101**, 2070–2075 (2004).
22. J. N. Sleigh, A. M. Rossor, A. D. Fellows, A. P. Tosolini, G. Schiavo, Axonal transport and neurological disease. *Nat. Rev. Neurol.* **15**, 691–703 (2019).
23. Q. Li, K. F. Tseng, S. J. King, W. Qiu, J. Xu, A fluid membrane enhances the velocity of cargo transport by small teams of kinesin-1. *J. Chem. Phys.* **148**, 123318 (2018).
24. R. Jiang *et al.*, Microtubule binding kinetics of membrane-bound kinesin-1 predicts high motor copy numbers on intracellular cargo. *Proc. Natl. Acad. Sci. U.S.A.* **116**, 26564–26570 (2019).
25. S. Pyrpassopoulos, H. Shuman, E. M. Ostap, Method for measuring single-molecule adhesion forces and attachment lifetimes of protein-membrane interactions. *Methods Mol. Biol.* **1046**, 389–403 (2013).
26. B. B. McIntosh, E. L. Holzbaur, E. M. Ostap, Control of the initiation and termination of kinesin-1-driven transport by myosin-Ic and nonmuscle tropomyosin. *Curr. Biol.* **25**, 523–529 (2015).
27. D. Beckers, D. Urbancic, E. Sezgin, Impact of nanoscale hindrances on the relationship between lipid packing and diffusion in model membranes. *J. Phys. Chem. B* **124**, 1487–1494 (2020).
28. J. Xu, S. J. King, M. Lapierre-Landry, B. Nemec, Interplay between velocity and travel distance of kinesin-based transport in the presence of tau. *Biophys. J.* **105**, L23–L25 (2013).
29. R. Grover *et al.*, Transport efficiency of membrane-anchored kinesin-1 motors depends on motor density and diffusivity. *Proc. Natl. Acad. Sci. U.S.A.* **113**, E7185–E7193 (2016).
30. C. Herold, C. Leduc, R. Stock, S. Diez, P. Schwille, Long-range transport of giant vesicles along microtubule networks. *Chemphyschem* **13**, 1001–1006 (2012).
31. S. R. Nelson, K. M. Trybus, D. M. Warshaw, Motor coupling through lipid membranes enhances transport velocities for ensembles of myosin Va. *Proc. Natl. Acad. Sci. U.S.A.* **111**, E3986–E3995 (2014).
32. K. Svoboda, S. M. Block, Force and velocity measured for single kinesin molecules. *Cell* **77**, 773–784 (1994).
33. J. Xu *et al.*, Casein kinase 2 reverses tail-independent inactivation of kinesin-1. *Nat. Commun.* **3**, 754 (2012).
34. Q. Li, S. J. King, A. Gopinathan, J. Xu, Quantitative determination of the probability of multiple-motor transport in bead-based assays. *Biophys. J.* **110**, 2720–2728 (2016).
35. E. M. Jones *et al.*, Interaction of tau protein with model lipid membranes induces tau structural compaction and membrane disruption. *Biochemistry* **51**, 2539–2550 (2012).
36. D. P. McVicker, L. R. Chrin, C. L. Berger, The nucleotide-binding state of microtubules modulates kinesin processivity and the ability of Tau to inhibit kinesin-mediated transport. *J. Biol. Chem.* **286**, 42873–42880 (2011).
37. S. Klumpp, R. Lipowsky, Cooperative cargo transport by several molecular motors. *Proc. Natl. Acad. Sci. U.S.A.* **102**, 17284–17289 (2005).
38. J. O. Wilson, A. D. Zaragoza, J. Xu, Tuning ensemble-averaged cargo run length via fractional change in mean kinesin number. *Phys. Biol.* **18**, 046004 (2021).
39. M. D. Stone *et al.*, Chirality sensing by Escherichia coli topoisomerase IV and the mechanism of type II topoisomerases. *Proc. Natl. Acad. Sci. U.S.A.* **100**, 8654–8659 (2003).
40. S. Liu *et al.*, A viral packaging motor varies its DNA rotation and step size to preserve subunit coordination as the capsid fills. *Cell* **157**, 702–713 (2014).
41. J. Huang, J. T. Buboltz, G. W. Feigenson, Maximum solubility of cholesterol in phosphatidylcholine and phosphatidylethanolamine bilayers. *Biochim. Biophys. Acta* **1417**, 89–100 (1999).
42. A. Parker, K. Miles, K. H. Cheng, J. Huang, Lateral distribution of cholesterol in dioleoylphosphatidylcholine lipid bilayers: Cholesterol-phospholipid interactions at high cholesterol limit. *Biophys. J.* **86**, 1532–1544 (2004).
43. A. R. Rogers, J. W. Driver, P. E. Constantinou, D. Kenneth Jamison, M. R. Diehl, Negative interference dominates collective transport of kinesin motors in the absence of load. *Phys. Chem. Chem. Phys.* **11**, 4882–4889 (2009).
44. J. Xu, Z. Shu, S. J. King, S. P. Gross, Tuning multiple motor travel via single motor velocity. *Traffic* **13**, 1198–1205 (2012).
45. N. D. Derr *et al.*, Tug-of-war in motor protein ensembles revealed with a programmable DNA origami scaffold. *Science* **338**, 662–665 (2012).
46. K. Furuta *et al.*, Measuring collective transport by defined numbers of processive and nonprocessive kinesin motors. *Proc. Natl. Acad. Sci. U.S.A.* **110**, 501–506 (2013).
47. S. R. Norris *et al.*, A method for multiprotein assembly in cells reveals independent action of kinesins in complex. *J. Cell Biol.* **207**, 393–406 (2014).
48. C. Leduc *et al.*, Cooperative extraction of membrane nanotubes by molecular motors. *Proc. Natl. Acad. Sci. U.S.A.* **101**, 17096–17101 (2004).
49. N. Hirokawa *et al.*, Submolecular domains of bovine brain kinesin identified by electron microscopy and monoclonal antibody decoration. *Cell* **56**, 867–878 (1989).
50. J. M. Scholey, J. Heuser, J. T. Yang, L. S. Goldstein, Identification of globular mechanochemical heads of kinesin. *Nature* **338**, 355–357 (1989).
51. L. Amos, A. Klug, Arrangement of subunits in flagellar microtubules. *J. Cell Sci.* **14**, 523–549 (1974).
52. M. H. Hinrichs *et al.*, Tau protein diffuses along the microtubule lattice. *J. Biol. Chem.* **287**, 38559–38568 (2012).
53. D. P. McVicker, G. J. Hoeprich, A. R. Thompson, C. L. Berger, Tau interconverts between diffusive and stable populations on the microtubule surface in an isoform and lattice specific manner. *Cytoskeleton* **71**, 184–194 (2014).
54. J. D. Knight, M. G. Lerner, J. G. Marcano-Velazquez, R. W. Pastor, J. J. Falke, Single molecule diffusion of membrane-bound proteins: Window into lipid contacts and bilayer dynamics. *Biophys. J.* **99**, 2879–2887 (2010).
55. F. A. Thomas, I. Visco, Z. Petrasek, F. Heinemann, P. Schwille, Diffusion coefficients and dissociation constants of enhanced green fluorescent protein binding to free standing membranes. *Data Brief* **5**, 537–541 (2015).
56. J. L. Stern, D. V. Lessard, G. J. Hoeprich, G. A. Morfini, C. L. Berger, Phosphoregulation of Tau modulates inhibition of kinesin-1 motility. *Mol. Biol. Cell* **28**, 1079–1087 (2017).
57. B. Y. Monroy *et al.*, Competition between microtubule-associated proteins directs motor transport. *Nat. Commun.* **9**, 1487 (2018).
58. C. Lebrand *et al.*, Late endosome motility depends on lipids via the small GTPase Rab7. *EMBO J.* **21**, 1289–1300 (2002).

59. E. B. Neufeld *et al.*, The ABCA1 transporter modulates late endocytic trafficking: Insights from the correction of the genetic defect in Tangier disease. *J. Biol. Chem.* **279**, 15571–15578 (2004).
60. D. R. Klopfenstein, M. Tomishige, N. Stuurman, R. D. Vale, Role of phosphatidylinositol(4,5)bisphosphate organization in membrane transport by the Unc104 kinesin motor. *Cell* **109**, 347–358 (2002).
61. S. E. Encalada, L. Szpankowski, C. H. Xia, L. S. Goldstein, Stable kinesin and dynein assemblies drive the axonal transport of mammalian prion protein vesicles. *Cell* **144**, 551–565 (2011).
62. J. Kerssemakers, J. Howard, H. Hess, S. Diez, The distance that kinesin-1 holds its cargo from the microtubule surface measured by fluorescence interference contrast microscopy. *Proc. Natl. Acad. Sci. U.S.A.* **103**, 15812–15817 (2006).
63. G. Woehlke *et al.*, Microtubule interaction site of the kinesin motor. *Cell* **90**, 207–216 (1997).
64. G. Skiniotis *et al.*, Modulation of kinesin binding by the C-termini of tubulin. *EMBO J.* **23**, 989–999 (2004).
65. B. J. Grant *et al.*, Electrostatically biased binding of kinesin to microtubules. *PLoS Biol.* **9**, e1001207 (2011).
66. W. H. Liang *et al.*, Microtubule defects influence kinesin-based transport in vitro. *Biophys. J.* **110**, 2229–2240 (2016).
67. E. P. Karasmanis *et al.*, Polarity of neuronal membrane traffic requires sorting of kinesin motor cargo during entry into dendrites by a microtubule-associated septin. *Dev. Cell* **46**, 518–524 (2018).
68. M. W. Gramlich *et al.*, Single molecule investigation of kinesin-1 motility using engineered microtubule defects. *Sci. Rep.* **7**, 44290 (2017).
69. M. Metivier *et al.*, Dual control of kinesin-1 recruitment to microtubules by Ensconsin in Drosophila neuroblasts and oocytes. *Development* **146**, dev171579 (2019).
70. P. J. Hooikaas *et al.*, MAP7 family proteins regulate kinesin-1 recruitment and activation. *J. Cell Biol.* **218**, 1298–1318 (2019).
71. K. Chiba, K. M. Ori-McKenney, S. Niwa, R. J. McKenney, Reconstitution of Kinesin-1 Activation. bioRxiv [Preprint] (2021). https://doi.org/10.1101/2021.03.12.434960 (Accessed date 30 May 2022).
72. J. C. Larcher, D. Boucher, S. Lazereg, F. Gros, P. Denoulet, Interaction of kinesin motor domains with alpha- and beta-tubulin subunits at a tau-independent binding site. Regulation by polyglutamylation. *J. Biol. Chem.* **271**, 22117–22124 (1996).
73. G. Liao, G. G. Gundersen, Kinesin is a candidate for cross-bridging microtubules and intermediate filaments. Selective binding of kinesin to detyrosinated tubulin and vimentin. *J. Biol. Chem.* **273**, 9797–9803 (1998).
74. Y. Konishi, M. Setou, Tubulin tyrosination navigates the kinesin-1 motor domain to axons. *Nat. Neurosci.* **12**, 559–567 (2009).
75. N. Kaul, V. Soppina, K. J. Verhey, Effects of alpha-tubulin K40 acetylation and detyrosination on kinesin-1 motility in a purified system. *Biophys. J.* **106**, 2636–2643 (2014).
76. T. E. Smith *et al.*, Single-molecule inhibition of human kinesin by adociasulfate-13 and -14 from the sponge Cladocroce aculeata. *Proc. Natl. Acad. Sci. U.S.A.* **110**, 18880–18885 (2013).
77. J. Howard, A. J. Hudspeth, R. D. Vale, Movement of microtubules by single kinesin molecules. *Nature* **342**, 154–158 (1989).
78. T. Ozeki *et al.*, Surface-bound casein modulates the adsorption and activity of kinesin on SiO2 surfaces. *Biophys. J.* **96**, 3305–3318 (2009).
79. M. Y. Jiang, M. P. Sheetz, Cargo-activated ATPase activity of kinesin. *Biophys. J.* **68**, 283S–284S, discussion 285S (1995).
80. D. L. Coy, W. O. Hancock, M. Wagenbach, J. Howard, Kinesin's tail domain is an inhibitory regulator of the motor domain. *Nat. Cell Biol.* **1**, 288–292 (1999).
81. M. Mikhaylova *et al.*, Resolving bundled microtubules using anti-tubulin nanobodies. *Nat. Commun.* **6**, 7933 (2015).
82. M. T. Gyparaki *et al.*, Tau forms oligomeric complexes on microtubules that are distinct from tau aggregates. *Proc. Natl. Acad. Sci. U.S.A.* **118**, e2021461118 (2021).
83. B. C. Carter, G. T. Shubeita, S. P. Gross, Tracking single particles: A user-friendly quantitative evaluation. *Phys. Biol.* **2**, 60–72 (2005).